AGU PUBLICATIONS

JGR

Journal of Geophysical Research: Atmospheres

RESEARCH ARTICLE

10.1002/2013JD021120

Key Points:
- Direct measurement of tsunami generated gravity waves in the thermosphere
- Gravity wave arrival azimuth determined from GOCE measurements
- Definition of a marker of thermospheric gravity waves inside GOCE data

Correspondence to:
R. F. Garcia,
Raphael.GARCIA@isae.fr

Citation:
Garcia, R. F., E. Doornbos, S. Bruinsma, and H. Hebert (2014), Atmospheric gravity waves due to the Tohoku-Oki tsunami observed in the thermosphere by GOCE, *J. Geophys. Res. Atmos.*, *119*, doi:10.1002/2013JD021120.

Received 31 OCT 2013
Accepted 24 MAR 2014
Accepted article online 31 MAR 2014

Atmospheric gravity waves due to the Tohoku-Oki tsunami observed in the thermosphere by GOCE

Raphael F. Garcia[1,2], Eelco Doornbos[3], Sean Bruinsma[4], and Hélène Hebert[5]

[1]ISAE, Toulouse, France, [2]Université de Toulouse, UPS-OMP, IRAP, Toulouse, France, [3]Faculty of Aerospace Engineering, TU Delft, Delft, Netherlands, [4]Department of Terrestrial and Planetary Geodesy, CNES, Toulouse, France, [5]CEA, DAM, DIF, Bruyères le Chatel, France

Abstract Oceanic tsunami waves couple with atmospheric gravity waves, as previously observed through ionospheric and airglow perturbations. Aerodynamic velocities and density variations are computed from Gravity Field and Steady-State Ocean Circulation Explorer (GOCE) accelerometer and thruster data during Tohoku-Oki tsunami propagation. High-frequency perturbations of these parameters are observed during three expected crossings of the tsunami-generated gravity waves by the GOCE satellite. From theoretical relations between air density and vertical and horizontal velocities inside the gravity wave, we demonstrate that the measured perturbations are consistent with a gravity wave generated by the tsunami and provide a way to estimate the propagation azimuth of the gravity wave. Moreover, because GOCE measurements can constrain the wave polarization, a marker (noted C^3) of any gravity wave crossing by the GOCE satellite is constructed from correlation coefficients between the observed atmospheric state parameters. These observations validate a new observation tool of thermospheric gravity waves generated by tsunamis above the open ocean.

1. Introduction

Long period tsunami waves couple at the ocean surface with atmospheric gravity waves propagating upward in the atmosphere [*Lognonné et al.*, 1998; *Occhipinti et al.*, 2006; *Hickey et al.*, 2009]. Due to kinetic energy conservation and to the exponential density decrease in the atmosphere, these waves are amplified and generate significant perturbations in the thermosphere/ionosphere system [*Peltier and Hines*, 1976]. Electron density perturbations due to these gravity waves were observed in GPS data [*Artru et al.*, 2005; *Rolland et al.*, 2010; *Galvan et al.*, 2011, 2012; *Occhipinti et al.*, 2013], ionospheric doppler sounders [*Liu et al.*, 2006, 2011], and ionospheric correction of altimetric satellites [*Occhipinti et al.*, 2006]. Recently, the effect of these gravity waves on the nightside airglow was modeled [*Hickey et al.*, 2010] and observed [*Makela et al.*, 2011], adding a new way to detect tsunami propagation in the thermosphere.

In this study, we demonstrate that accelerometer data from the GOCE (Gravity Field and Steady-State Ocean Circulation Explorer) satellite observed the gravity waves generated by the Tohoku-Oki tsunami (on 11 March 2011). The very low Earth orbit of the GOCE mission, at 270 km altitude, its drag compensated platform, and the unprecedented quality of its accelerometers [*Floberghagen et al.*, 2011] allow us to recover very precisely the nongravitational forces exerted on the satellite and deduce air density and winds in the thermosphere along the satellite track [*Doornbos et al.*, 2010]. The nongravitational accelerations of the satellite are known to within 2×10^{-12} m/s^2 [*Floberghagen et al.*, 2011]. The density and wind retrieval along satellite track have an uncertainty smaller than 1% and are provided with ten seconds sampling. Recently, *Garcia et al.* [2013] demonstrated that GOCE detected the infrasound created by the seismic waves of the same event. The analysis of GOCE data is pursued here in order to detect atmospheric perturbations due to the open ocean surface displacements generated by the tsunami. We first identify the expected windows in which GOCE crosses the tsunami-generated gravity wave and present the high-frequency perturbations in these windows. Then, a monochromatic plane wave analysis demonstrates that the aerodynamic velocities and air density perturbations are consistent with gravity waves created by the Tohoku-Oki tsunami. Finally, a marker of any gravity wave signal in GOCE data is designed by using expected correlations between aerodynamic velocities and time derivative of air density.

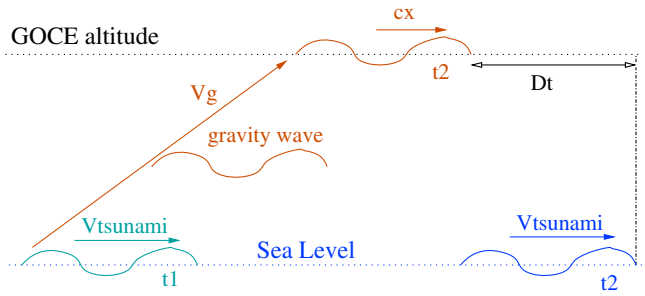

Figure 1. Scheme of tsunami and gravity wave propagation in the vertical plane along tsunami propagation direction (hereafter noted as *x*). The time of the gravity wave excitation by the tsunami is *t*1. The time of gravity wave arrival at the GOCE altitude (after about 1 h) is *t*2. Tsunami position at this time is provided on the right of the figure. Vg stands for the gravity wave group velocity and Dt is the time delay between the arrival of the tsunami wave at the ocean surface and the arrival of the gravity wave above that point at the altitude of GOCE. Adapted from *Occhipinti et al.* [2013].

2. Observations of Atmospheric Gravity Waves Generated by Tohoku-Oki Tsunami

2.1. Identification of Expected Signals

The propagation time of the tsunami at the surface of the ocean is computed with Tsunami Travel Time (TTT) software [*Wessel*, 2009]. According to *Occhipinti et al.* [2013], the horizontal and vertical gravity wave propagation from the ocean surface to the altitude of GOCE should be computed by taking into account the gravity wave dominant period and the altitude of the satellite. Figure 1 presents a scheme of the tsunami and associated gravity wave propagations. Gravity wave propagates in the atmosphere at group velocity Vg and horizontal phase velocity c_x, whereas the tsunami wave propagates at velocity V_{tsunami} on the ocean surface. The propagation time between the ocean surface and the GOCE altitude ($t2 - t1$) is about 1 h. In this case, the time delay (Dt) between the arrival of the tsunami wave at some point of the ocean surface and the arrival of the gravity wave at the altitude of GOCE above that point is fixed to 240 s, corresponding to the propagation of a gravity wave with a 10 min period up to the altitude of GOCE, according to *Occhipinti et al.* [2013]. However, the uncertainty on this number is large because a proper estimate would require a full modeling of the gravity wave propagation, including wind effects. Then, the crossing points between the satellite track and the gravity wave are selected assuming that the gravity wave signals last during 1600 s following the expected first arrival time. This time range is in between 1 and 3 dominant periods of the signal. Figure 2 presents the result of this analysis for GOCE orbits following the Tohoku event. Three gravity wave crossing events are obtained on three consecutive ascending orbits following the earthquake.

2.2. GOCE Acceleration and Thruster Data

Figure 3 presents the high-frequency perturbations of thruster and aerodynamic accelerations measured during the three gravity wave crossing events. The high-frequency variations of thruster and Z and Y components of aerodynamic acceleration are obtained in the same way by subtracting a low-pass filtered version of the original signal with 650 s corner frequency or ≈1/8 of the orbit period. However, because of large amplitude high-frequency variations of the *Y* component of the aerodynamic acceleration at the pole, high-frequency variations of this signal are obtained by substracting a polynomial fit of order 7 along ±50° latitude ascending branches. The crossing windows identified from the previous analysis present high-frequency variations of thruster and aerodynamic accelerations above the noise level in these mid-latitude regions. However, these perturbations arrive at the satellite earlier than expected. We ascribe this arrival time discrepancy to the strong thermospheric winds blowing eastward and southward. A simple estimation of the wind effect is computed by taking into account the observation geometry (see Figure 4) and the wave parameters listed in Table 1 and assuming average wind and atmospheric parameters between 140 km altitude and GOCE's position. This minimum value of the wavefront shift due to wind is estimated to 241 km along the GOCE orbit, corresponding to an arrival on the GOCE data 30 s earlier than expected at the first gravity wave crossing.

2.3. Monochromatic Plane Wave Analysis

In the following we assume that the atmospheric gravity waves generated by tsunamis far from the seismic source can be fairly well approximated by a monochromatic plane wave excited by the movement of a tsunami wave of dominant period T_w propagating along *x* direction. Under such an assumption, the gravity wave propagation from the ocean surface to the thermosphere can be described in two dimensions

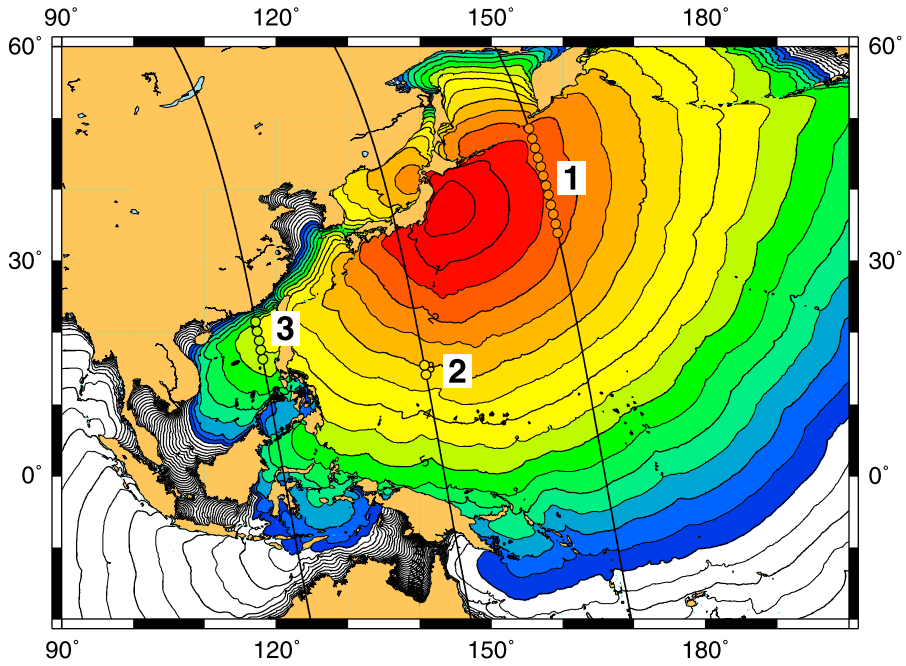

Figure 2. Expected crossing points (circles) between GOCE tracks and the gravity waves generated by the tsunami. Contour lines and color code represent the propagation time of the tsunami at the ocean surface computed by TTT (thick lines every hour). Circles filled with the tsunami propagation time color code are superimposed on the satellite tracks (black lines) in order to indicate the gravity wave crossing areas. The three crossing events are numbered in chronological order.

(coordinates x and z). The vertical winds are neglected, but horizontal winds along x direction (u_{0x}) are included in our analysis. The velocity perturbations (U_x and U_z), the pressure perturbations (P), and density perturbations (ρ) are related to the background wind (u_{0x}) and background density (ρ_0) by the following equations, assuming incompressibility [*Nappo*, 2002]:

$$\frac{\partial U_x}{\partial t} + u_{0x}\frac{\partial U_x}{\partial x} = -\frac{1}{\rho_0}\frac{\partial P}{\partial x} \tag{1}$$

$$\frac{\partial U_z}{\partial t} + u_{0x}\frac{\partial U_z}{\partial x} = -\frac{1}{\rho_0}\frac{\partial P}{\partial z} - \frac{\rho}{\rho_0}g \tag{2}$$

$$\frac{\partial U_x}{\partial x} + \frac{\partial U_z}{\partial z} = 0 \tag{3}$$

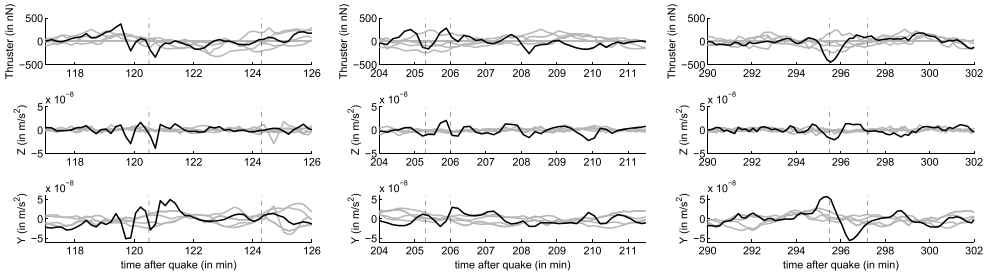

Figure 3. (left to right) Signals at the three crossing windows (dashed lines) identified by the previous analysis. (top to bottom) High-frequency variations of GOCE thruster (in nanonewton) and spacecraft body-fixed Z and Y components of aerodynamic accelerations (in meter per second squared). Black lines are signals along ascending branches corresponding to the three crossing events. Grey lines are signals for three ascending branches before and two after the crossing events.

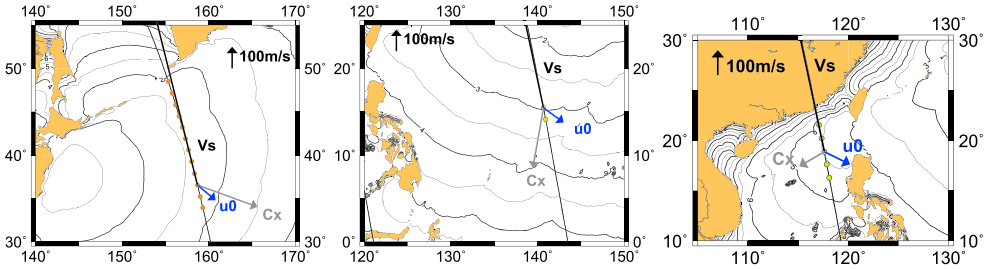

Figure 4. (left to right) Close up on the geometry of the crossing events 1, 2, and 3, indicated in Figure 1. Satellite velocity ($Vs \approx 7.8$ km/s, in black) is plotted with the gravity wave horizontal phase velocity (c_x, in grey) and the background wind at the altitude of GOCE satellite (u_0, in blue). See Table 1 for details. Contours of tsunami arrival time at ocean surface are also indicated.

$$\frac{\partial \rho}{\partial t} + u_{0x}\frac{\partial \rho}{\partial x} + U_z\frac{\partial \rho_0}{\partial z} = 0 \tag{4}$$

where g is the gravity acceleration. We ensure that the incompressibility assumption is valid by comparing, later in the text, the vertical wave numbers to the inverse of atmospheric scale height [*Lighthill*, 2001]. The ratio of these two quantities is on the order of 2 which satisfies the "larger than one" condition but suggests that compressibility should be taken into account in future work. Assuming that the atmosphere can be considered locally as isothermal and with constant background wind along x direction, the background density ρ_0 decreases exponentially with scale height H and u_{0x} is constant. Then, a solution of these equations is derived by assuming that the perturbation variables (U_x, U_z, P, and ρ) are the product of a complex amplitude term by a monochromatic plane wave complex exponential of the form $\exp[i(k_x x + k_z z - \omega t)]$. The two components of the wave vector are k_x and k_z, and $\omega = \frac{2\pi}{T_w}$ is the wave angular frequency. After some obvious manipulations, we obtain the gravity wave dispersion relation in a constant background wind and isothermal atmosphere [*Nappo*, 2002]

$$\frac{N^2}{\Omega^2} = 1 + \frac{k_z^2}{k_x^2} \tag{5}$$

where $\Omega = \omega - k_x u_{0x}$ is the intrinsic frequency of gravity wave, $N = \sqrt{\frac{\gamma-1}{\gamma}\frac{g}{H}}$ is the Brunt-Väisälä frequency, and γ is the usual ratio of specific heats. In our case, the angular frequency ω is fixed by the dominant period (T_w) of the tsunami forcing the ocean surface through the following relation $\omega = \frac{2\pi}{T_w}$. It remains constant along the vertical propagation of the wave.

In addition, we obtain the following simple relation between the amplitudes of horizontal and vertical velocities inside the gravity wave:

$$U_z = -\frac{k_x}{k_z}U_x \tag{6}$$

From equation (4), we can also relate the vertical velocities to the horizontal derivative of density perturbations by the following expression:

$$U_z = -\frac{\Omega H}{k_x}\frac{1}{\rho_0}\frac{\partial \rho}{\partial x} \tag{7}$$

and so

$$U_x = \frac{\Omega H}{k_z}\frac{1}{\rho_0}\frac{\partial \rho}{\partial x} \tag{8}$$

Table 1. Wave and Geometry Parameters of Each Gravity Wave Crossing by GOCE

Crossing Number	T_w (min)	k_x Azimuth Φ_w (deg)	T_A (s)	u_0 Zonal	Meridional (m/s)	λ_x (km)	c_x (m/s)	k_z (rad/m)
1	10	110	40	92	−56	177	295	−3.94e-5
2	25	190	55	100	−59	423	282	−3.87e-5
3	35	240	90	104	−47	244	116	−4.83e-5

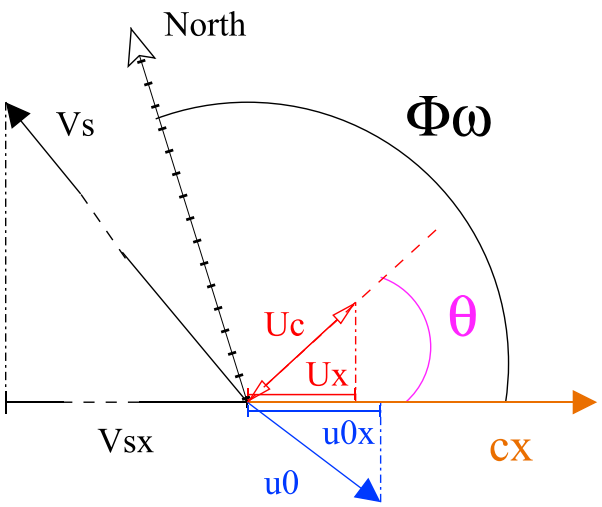

Figure 5. Observation geometry in the horizontal plane, aligned with the direction of propagation of the gravity wave generated by the tsunami. The satellite velocity (V_S) is not to scale. The horizontal phase velocity of the gravity wave, the horizontal wind, and the cross-track wind velocity measured by GOCE are c_x, u_0, and U_c, respectively. The angles between gravity wave propagation direction and cross-track direction and northward direction are θ and Φ_w.

Equations (6), (7), and (8) should be verified by the air density and aerodynamic velocities obtained from GOCE measurements if the measured perturbations are due to the gravity wave generated by the tsunami. However, possible discrepancies with measurements could be ascribed to the assumptions used to obtain these equations: plane wave propagation, no attenuation, and free propagation far from the gravity wave source. Future numerical studies should include 3-D spherical geometry, attenuation and wind effects, and bottom forcing by the propagating tsunami wave in order to reproduce the waveforms of observed air density and velocity variations.

2.4. Application to GOCE Data

Figure 4 shows the observation geometry of the three crossings, indicating the satellite horizontal velocity (V_S), the horizontal phase velocity of the gravity wave (c_x), and the background wind direction (u_0) at the altitude of GOCE. Figure 5 defines all the parameters in the horizontal plane for a geometry corresponding to the first crossing window. V_S (≈7.8 km/s) is more than 1 order of magnitude larger than both c_x and u_0. In order to demonstrate that the measured perturbations of air density and aerodynamic velocities verify equations (6), (7), and (8), the monochromatic plane wave parameters should be estimated. To do so, the Brunt-Väisälä frequency and atmospheric scale height are estimated, respectively, to $N^2 \approx 1.10^{-4}$ rad^2/s^2 and $H \approx 43.5$ km from the NRLMSISE-00 model [*Picone et al.*, 2002] at the time and location of the first crossing with GOCE satellite, and with the following input parameters: 81 day average of $F_{10.7} = 106.7$, daily $F_{10.7} = 131$ and AP = 37. The background wind (u_0) is obtained from HWM93 [*Hedin et al.*, 1996]. The dominant period T_w of the tsunami and its propagation direction are extracted from numerical simulations of the tsunami at the ocean surface [*Hébert et al.*, 2001]. Then the horizontal wave vector k_x should be estimated. To do so, the time variable of GOCE data (t_d) is linked to the x coordinate along the gravity wave propagation direction by the formula $x = V^r_{Sx} t_d$ where V^r_{Sx} is the projection along x of the velocity of GOCE relative to the wavefront. With such relation, the apparent period of observed perturbations (T_A) can be used to determine the horizontal wavelength of the wave: $\lambda_x = V^r_{Sx} T_A$, and the horizontal wave vector $k_x = \frac{2\pi}{\lambda_x}$. The satellite velocity relative to the wavefront is

$$V^r_{Sx} = V_{Sx} - u_{0x} - c_x \tag{9}$$

where V_{Sx}, u_{0x}, and c_x are, respectively, the satellite velocity and the background wind in the direction of wave propagation (x) and the gravity wave phase velocity. The horizontal phase velocity depends on the intrinsic period (Ω), which is fixed by the tsunami wave period (T_w), and horizontal wave number (k_x). Because $V_S >> c_x$, unless the satellite orbit is almost exactly perpendicular to the wave propagation direction, we can consider $V_{Sx} >> c_x$ and estimate the horizontal wavelength neglecting c_x in a first step. Then c_x is computed, and the process is iterated. So horizontal phase velocity and horizontal wave number are determined iteratively, starting with zero phase velocity, estimating V^r_{Sx}, then k_x from T_A, and finally c_x from the dispersion relation, and repeating the process. The iteration process quickly converges to values presented in Table (1). Using equation (5), the vertical wave numbers are also estimated. Amplitudes are about twice the inverse of atmospheric scale height ($\frac{1}{H} = 2.29e-5$ m^{-1}), ensuring that the incompressibility assumption is approximately satisfied.

Once the monochromatic plane wave parameters have been estimated, relations (6) and (7) are used to produce synthetic vertical velocities expected for a gravity wave generated by the tsunami from horizontal

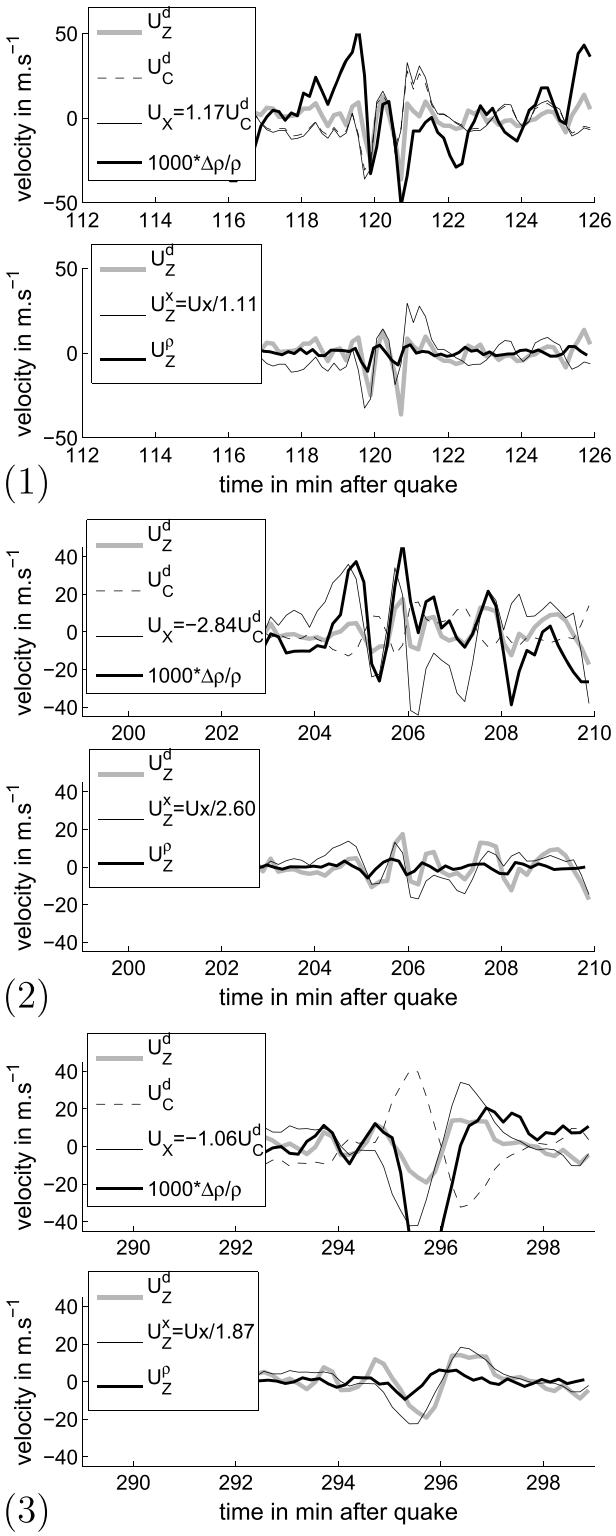

Figure 6. Crossing events 1, 2, and 3. (top) For each event, velocities and relative density variations deduced from GOCE accelerations and thruster data. (bottom) Comparison between vertical velocity deduced from GOCE accelerations (grey line) and synthetic vertical velocities deduced from horizontal velocity (thin black line) and from density variations (thick black line).

velocity along x and from density variations measured by GOCE according to

$$U_z^x(t_d) = -\frac{k_x}{k_z} U_x^d(t_d) \tag{10}$$

and

$$U_z^\rho(t_d) = -\frac{\Omega H}{k_x V_{sx}^r} \frac{\partial \Delta\rho^d/\rho}{\partial t_d}(t_d) \tag{11}$$

where $U_x^d(t_d)$ and $\frac{\Delta\rho^d}{\rho}(t_d)$ are, respectively, the projection along x of the horizontal velocity perturbation and the relative density variations measured by GOCE.

2.5. Validation of the Tsunami Gravity Wave Detection

The aerodynamic velocity is defined as the velocity of air particles with respect to the satellite. Its component in the cross-track direction (U_C^d) and air density (ρ^d) are obtained simultaneously by an analysis of GOCE accelerations and thruster data in the horizontal plane following *Doornbos et al.* [2010]. The same algorithm is repeated along a vertical plane to estimate simultaneously the upward aerodynamic velocity (U_z^d) and air density (ρ^d). Then, assuming that U_C^d is the projection in cross-track direction of the horizontal velocity along the wave propagation direction U_x^d, these two velocities are related through $U_x^d = \frac{U_C^d}{\cos(\theta)}$, where θ is the angle between the cross-track direction and the tsunami gravity wave propagation direction. The high-frequency variations of these parameters are obtained according to the process described above.

Figure 6 presents high-frequency perturbations of aerodynamic velocities and relative density at the three gravity wave crossing times. The three input measurements (U_C^d, U_z^d, and $\frac{\Delta\rho^d}{\rho}$) present different amplitudes and phases. In particular, the relative density perturbations present frequencies lower than aerodynamic velocities and are not in phase with velocities. However, the synthetic vertical velocities (U_z^x and U_z^ρ), computed assuming that these waves were produced by the tsunami, are consistent both in phase and in amplitude (within a

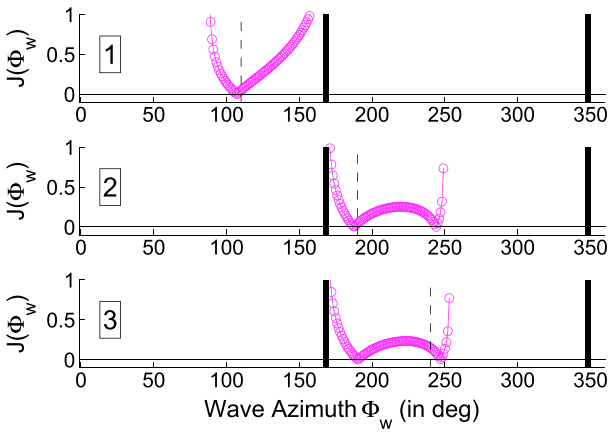

Figure 7. Cost function ($J(\Phi_w)$, open circles) for the three gravity wave crossing events as a function of gravity wave propagation azimuth (Φ_w, in degrees). Vertical dashed lines indicate expected values listed in Table 1. Vertical thick lines indicate singularities due to gravity wave propagation along GOCE orbit.

factor 2) between them and with the vertical velocities measured by GOCE. This consistency demonstrates that these waves were created by the tsunami wave at the ocean surface.

2.6. Determination of the Gravity Wave Propagation Direction

From equations (10), (11), and relations between the various parameters in the plane wave analysis, if we assume that the tsunami period and atmospheric parameters are known, the amplitude ratio $\frac{U_z^d}{U_C^d}$ can be used to constrain the azimuth of the gravity wave propagation direction (Φ_w). To do so, we repeated the above analysis by varying the arrival azimuth of the wave between 0° and 360° and plotting the logarithm of data to theoretical $\frac{U_z^d}{U_C^d}$ amplitude ratios defined by the following:

$$J(\Phi_w) = \left| \log 10 \left(\left| \frac{U_z^d}{U_C^d} \Big/ \frac{-k_x}{k_z \cos(\theta)} \right| \right) \right| \tag{12}$$

when this parameter is zero, the measured and theoretical amplitude ratios are equal. Due to the projection of U_x on the cross-track direction, the horizontal velocities inside the wave cannot be estimated when the tsunami is propagating exactly along the GOCE track, which corresponds to θ values of 90° and 270°, or Φ_w values around 170° and 350°. The following additional constraints allow restricting the parameter space of Φ_w consistent with a gravity wave propagation: data and theoretical $\frac{U_z^d}{U_C^d}$ amplitude ratios have the same sign, or $\frac{U_z^d}{U_C^d} \Big/ \frac{-k_x}{k_z \cos(\theta)} > 0$; Ω is positive (necessary for gravity wave propagation); k_z is real (necessary for gravity wave propagation); data and theoretical $\frac{U_z^d}{\frac{\partial \Delta \rho^d / \rho}{\partial t_d}}$ amplitude ratios have the same sign, or $\frac{U_z^d}{\frac{\partial \Delta \rho^d / \rho}{\partial t_d}} \Big/ \frac{-\Omega H}{k_x V_{sx}^f} > 0$.

After excluding the azimuth range values for which the above conditions are not fulfilled, the results for the three crossing events are presented in Figure 7. The first crossing event presents a single minimum close to the expected azimuth. The other two crossings present two minimum values, and the expected azimuth is close by to one of them in both cases. This exercise demonstrates that knowing the tsunami forcing period and atmospheric state parameters, the propagation azimuth of the atmospheric gravity wave can be constrained, thanks to the vertical to cross-track velocities amplitude ratio.

3. Definition of a Simple Marker of Gravity Waves Inside GOCE Data: C^3

From the plane wave analysis presented before, we deduce that when GOCE crosses a gravity wave, cross-track aerodynamic velocity, vertical aerodynamic velocity, and time derivative of air density perturbations should be correlated. Consequently, we define a simple marker of these correlations inside GOCE data by computing the absolute value of the product between the three correlation coefficients

$$C^3 = \left| \mathrm{CC}(U_C; Uz) \times \mathrm{CC}(U_C; \frac{d(\Delta\rho/\rho)}{dt}) \times \mathrm{CC}(Uz; \frac{d(\Delta\rho/\rho)}{dt}) \right| \tag{13}$$

where $\mathrm{CC}(f, g)(t_d)$ is the correlation coefficient between functions f and g over a given window length at time t_d centered on this window. In this computation, the high-frequency relative density perturbations are computed as described above, and the high-frequency variations of aerodynamic velocities are obtained by simply removing a trend inside each correlation window before computing the correlation coefficient. When GOCE is crossing a gravity wave, C^3 should be close to 1 and 0 from random perturbations. In particular, C^3 decreases drastically as soon as one of the three correlation coefficients is far from ± 1.

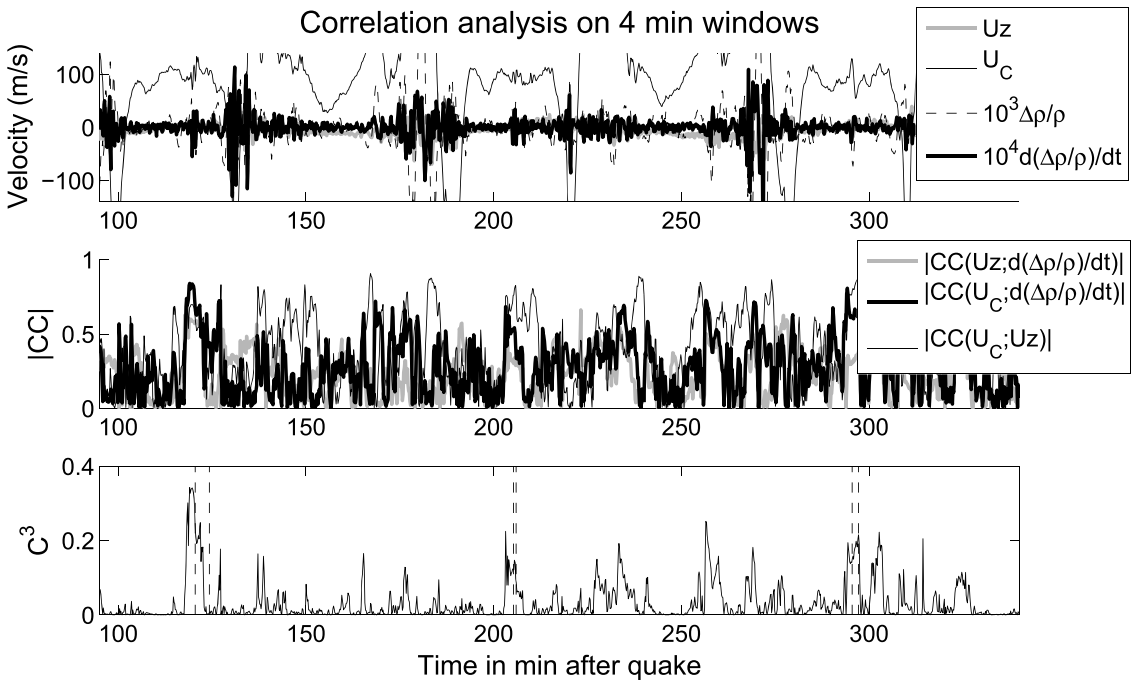

Figure 8. (top) Vertical (*Uz*) and cross-track (U_C) aerodynamic velocities (in meter per second) and high-frequency variations of the relative density (×1000) and its time derivative (×10 000). (middle) Absolute values of CC(U_C; *Uz*), $CC(U_C; \frac{d(\Delta\rho/\rho)}{dt})$, and $CC(Uz; \frac{d(\Delta\rho/\rho)}{dt})$ correlation coefficients. (bottom) C^3 marker. Correlation window is 4 min length. Vertical dashed lines indicate the tsunami gravity wave crossing windows.

Figure 8 presents the input data and C^3 computations during three orbits after the Tohoku event. C^3 presents values above 0.2 at the three crossing times with the tsunami-generated gravity wave, meaning that the logarithmic average of the three correlation coefficients is larger than 0.6. Another gravity wavefront may have been crossed 260 min after the quake on the other side of the planet during the descending branch. These waves are not related to the quake and tsunami, and this observation reveals the potential of C^3 marker for gravity wave detection.

4. Conclusions

High-frequency perturbations of GOCE accelerometer and thruster data were shown to be due to atmospheric gravity waves created by the Tohoku-Oki tsunami propagating in the Pacific Ocean. Our demonstration relies on the aerodynamic velocities and density perturbations computed from GOCE data and uses the theoretical relations between these parameters expected for gravity waves generated by the tsunami. Despite limitations due to the plane wave hypothesis and to assumptions on gravity wave excitation and propagation, the GOCE data are in agreement with these theoretical relations. In addition, if tsunami forcing frequency and atmospheric state parameters are known, aerodynamic velocities allow estimating the propagation azimuth of the tsunami-generated gravity wave. Moreover, a new marker of gravity wave signals inside GOCE data (C^3) is designed by the product of the three correlation coefficients computed between vertical and cross-track aerodynamic velocities and the time derivative of relative air density perturbations. This marker has the potential to detect any gravity wave signal inside GOCE data.

The detection of tsunami-generated gravity waves by GOCE provides a new observation tool for these waves. Compared to GPS ionospheric sounding and nightside airglow emissions, it is not limited by the integration along the line of sight, the complex response of the wave marker (either electron density or airglow emission) to the neutral wave, or the observation conditions related to the background ionosphere state. Future modeling studies of tsunami-generated gravity waves should include lateral atmospheric variations and background winds in order to properly reproduce the arrival times at the satellite altitude and the observed waveforms.

Acknowledgments
This study was funded by CNES/TOSCA through space research scientific projects and by ESA. We acknowledge Frédéric Nahan who started this analysis during his master's degree research training period at IRAP. The processing of GOCE data for retrieval of thermosphere density and wind data was funded by ESA's Support To Science Element (STSE) program.

References

Artru, J., V. Ducic, H. Kanamori, P. Lognonné, and M. Murakami (2005), Ionospheric detection of gravity waves induced by tsunamis, *Geophys. J. Int.*, *160*, 840–848.

Doornbos, E., J. van den Ijssel, H. Lühr, M. Förster, and G. Koppenwallner (2010), Neutral density and crosswind determination from arbitrarily oriented multi-axis accelerometers on satellites, *J. Spacecraft Rockets*, *47*, 580–589, doi:10.2514/1.48114.

Floberghagen, R., M. Fehringer, D. Lamarre, D. Muzi, B. Frommknecht, C. Steiger, J. Piñeiro, and A. da Costa (2011), Mission design, operation and exploitation of the gravity field and steady-state ocean circulation explorer mission, *J. Geod.*, *85*, 749–758, doi:10.1007/s00190-011-0498-3.

Galvan, D. A., A. Komjathy, M. P. Hickey, and A. J. Mannucci (2011), The 2009 Samoa and 2010 Chile tsunamis as observed in the ionosphere using GPS total electron content, *J. Geophys. Res.*, *116*, A06318, doi:10.1029/2010JA016204.

Galvan, D. A., A. Komjathy, M. P. Hickey, P. Stephens, J. Snively, Y. Tony Song, M. D. Butala, and A. J. Mannucci (2012), Ionospheric signatures of Tohoku-Oki tsunami of March 11, 2011: Model comparisons near the epicenter, *Radio Sci.*, *47*, RS4003, doi:10.1029/2012RS005023.

Garcia, R. F., S. Bruinsma, P. Lognonné, E. Doornbos, and F. Cachoux (2013), GOCE: The first seismometer in orbit around the Earth, *Geophys. Res. Lett.*, *40*, 1015–1020, doi:10.1002/grl.50205.

Hébert, H., P. Heinrich, F. Schindelé, and A. Piatanesi (2001), Far-field simulation of tsunami propagation in the Pacific Ocean: Impact on the Marquesas Islands (French Polynesia), *J. Geophys. Res.*, *106*, 9161–9177, doi:10.1029/2000JC000552.

Hedin, A. E., et al. (1996), Empirical wind model for the upper, middle and lower atmosphere, *J. Atmos. Terr. Phys.*, *58*, 1421–1447.

Hickey, M. P., G. Schubert, and R. L. Walterscheid (2009), Propagation of tsunami-driven gravity waves into the thermosphere and ionosphere, *J. Geophys. Res.*, *114*, A08304, doi:10.1029/2009JA014105.

Hickey, M. P., G. Schubert, and R. L. Walterscheid (2010), Atmospheric airglow fluctuations due to a tsunami-driven gravity wave disturbance, *J. Geophys. Res.*, *115*, A06308, doi:10.1029/2009JA014977.

Lighthill, J. (2001), *Waves in Fluids*, 520 pp., Cambridge Univ. Press, Cambridge, U. K.

Liu, J. Y., Y. B. Tsai, S. W. Chen, C. P. Lee, Y. C. Chen, H. Y. Yen, W. Y. Chang, and C. Liu (2006), Giant ionospheric disturbances excited by the M9.3 Sumatra earthquake of 26 December 2004, *Geophys. Res. Lett.*, *33*, L02103, doi:10.1029/2005GL023963.

Liu, J.-Y., C.-H. Chen, C.-H. Lin, H.-F. Tsai, C.-H. Chen, and M. Kamogawa (2011), Ionospheric disturbances triggered by the 11 March 2011 M9.0 Tohoku earthquake, *J. Geophys. Res.*, *116*, A06319, doi:10.1029/2011JA016761.

Lognonné, P., E. Clévédé, and H. Kanamori (1998), Normal mode summation of seismograms and barograms in a spherical earth with realistic atmosphere, *Geophys. J. Int.*, *135*, 388–406.

Makela, J. J., et al. (2011), Imaging and modeling the ionospheric airglow response over Hawaii to the tsunami generated by the Tohoku earthquake of 11 March 2011, *Geophys. Res. Lett.*, *38*, L00G02, doi:10.1029/2011GL047860.

Nappo, C. (2002), *An Introduction to Atmospheric Gravity Waves*, 276 pp., Academic Press, San Diego, Calif.

Occhipinti, G., P. Lognonné, E. Kherani, and H. Hébert (2006), Three-dimensional waveform modeling of ionospheric signature induced by the 2004 Sumatra tsunami, *Geophys. Res. Lett.*, *33*, L20104, doi:10.1029/2006GL026865.

Occhipinti, G., L. Rolland, P. Lognonné, and S. Watada (2013), From Sumatra 2004 to Tohoku-Oki 2011: The systematic GPS detection of the ionospheric signature induced by tsunamigenic earthquakes, *J. Geophys. Res. Space Physics*, *118*, 3626–3636, doi:10.1002/jgra.50322.

Peltier, W., and C. Hines (1976), On the possible detection of tsunamis by a monitoring of the ionosphere, *J. Geophys. Res.*, *81*, 1995–2000.

Picone, J. M., A. E. Hedin, D. P. Drob, and A. C. Aikin (2002), NRLMSISE-00 empirical model of the atmosphere: Statistical comparisons and scientific issues, *J. Geophys. Res.*, *107*(A12), 1468, doi:10.1029/2002JA009430.

Rolland, L. M., G. Occhipinti, P. Lognonné, and A. Loevenbruck (2010), Ionospheric gravity waves detected offshore Hawaii after tsunamis, *Geophys. Res. Lett.*, *37*, L17101, doi:10.1029/2010GL044479.

Wessel, P. (2009), Analysis of observed and predicted tsunami travel times for the Pacific and Indian oceans, *Pure Appl. Geophys.*, *166*, 301–324, doi:10.1007/s00024-008-0437-2.